Discovery of an orally active small-molecule irreversible inhibitor of protein disulfide isomerase for ovarian cancer treatment

Shili Xu[a], Alexey N. Butkevich[b], Roppei Yamada[a], Yu Zhou[c], Bikash Debnath[a], Roger Duncan[a], Ebrahim Zandi[c,d], Nicos A. Petasis[b,c,1], and Nouri Neamati[a,c,1]

[a]Department of Pharmacology and Pharmaceutical Sciences, School of Pharmacy, University of Southern California, Los Angeles, CA 90033; [b]Department of Chemistry and Loker Hydrocarbon Research Institute, Dornsife College, University of Southern California, Los Angeles, CA 90089; [c]Norris Comprehensive Cancer Center, Keck School of Medicine, University of Southern California, Los Angeles, CA 90033; and [d]Department of Molecular Microbiology and Immunology, Keck School of Medicine, University of Southern California, Los Angeles, CA 90033

Edited by Dennis A. Carson, University of California at San Diego, La Jolla, CA, and approved August 16, 2012 (received for review March 29, 2012)

Protein disulfide isomerase (PDI), an endoplasmic reticulum chaperone protein, catalyzes disulfide bond breakage, formation, and rearrangement. The effect of PDI inhibition on ovarian cancer progression is not yet clear, and there is a need for potent, selective, and safe small-molecule inhibitors of PDI. Here, we report a class of propynoic acid carbamoyl methyl amides (PACMAs) that are active against a panel of human ovarian cancer cell lines. Using fluorescent derivatives, 2D gel electrophoresis, and MS, we established that PACMA 31, one of the most active analogs, acts as an irreversible small-molecule inhibitor of PDI, forming a covalent bond with the active site cysteines of PDI. We also showed that PDI activity is essential for the survival and proliferation of human ovarian cancer cells. In vivo, PACMA 31 showed tumor targeting ability and significantly suppressed ovarian tumor growth without causing toxicity to normal tissues. These irreversible small-molecule PDI inhibitors represent an important approach for the development of targeted anticancer agents for ovarian cancer therapy, and they can also serve as useful probes for investigating the biology of PDI-implicated pathways.

oral bioavailability | drug resistance | BODIPY-conjugation

Ovarian cancer is one of the leading causes of death in women with gynecological cancers in the United States. About 70% of ovarian cancer cases are diagnosed at a late stage and therefore, poorly treatable (1). Although the current standard treatment for ovarian cancer involving the use of paclitaxel and carboplatin after aggressive surgical cytoreduction usually results in multiyear survival, prolonged use of platinum-based chemotherapy often induces drug resistance, which causes ovarian cancer relapse and eventually, death of patients (2). In this context, there is an urgent medical need for breakthrough drugs with effective therapeutic impact on ovarian cancer.

Protein disulfide isomerase (PDI) is a 57-kDa chaperone protein located in the endoplasmic reticulum (ER) (3). Acting as a thiol oxidoreductase, PDI catalyzes the formation, breakage, and rearrangement of disulfide bonds and therefore, regulates oxidative protein folding as well as cell viability (4, 5). Located in the two PDI active sites in the α- and α′-domains are two conserved cysteine residues within the CGHC motif, which are essential for the activity of PDI and the cycle between oxidized (disulfide) and reduced (dithiol) states (6). It has been reported that ER stress and unfolded protein response can activate PDI expression (7). Increased PDI levels have been documented in a variety of human cancers, including ovarian (8), prostate (9), and lung cancers (10, 11) as well as lymphoma (11), glioma (12, 13), acute myeloid leukemia (7), and melanoma (5, 14). Inhibition of PDI activity leads to apoptosis in cancer (5), suggesting that PDI is a promising druggable target. Moreover, small-molecule PDI inhibitors have been reported to inhibit HIV-1 entry into cells (15). Several small molecules were previously reported as selective irreversible PDI inhibitors that suppressed apoptosis caused by misfolded proteins in a model of Huntington disease (4). A peptide antibiotic, bacitracin, interacts with and inhibits PDI through disulfide bond formation with activity in the high micromolar range (16). Although bacitracin is widely used as a PDI inhibitor in research, its clinical use is hampered by its nephrotoxicity and low membrane permeability (17–19). Therefore, the development of safer and more effective small-molecule PDI inhibitors remains an attractive approach for cancer treatment.

Previously, we reported that a class of propynoic acid carbamoyl methyl amides (PACMAs) showed a broad spectrum of cytotoxicity in a panel of human cancer cell lines, with relatively selective potency in ovarian cancer cells resistant to doxorubicin and paclitaxel (20). Herein, we designed and synthesized a series of PACMA derivatives exhibiting significant cytotoxicity in human ovarian cancer. We also established that these small molecules act as potent irreversible PDI inhibitors. Among these molecules, PACMA **31** (bold numbers are used to indicate compounds) exhibited in vivo activity with oral bioavailability in a mouse xenograft model of human ovarian cancer. PACMA **31** is an orally active small-molecule PDI inhibitor with desirable pharmacological properties for cancer treatment. Most importantly, this study shows that PDI is a druggable target for cancer therapy, and it opens a promising area of research to develop treatments with a unique mechanism of action.

Results

PACMAs Show Cytotoxicity in a Panel of Ovarian Cancer Cell Lines. To establish more informative structure–activity relationships and gain key insights on the likely protein targets of PACMAs in cancer, we designed and synthesized a series of PACMA derivatives (*SI Materials and Methods*, Scheme **S1**, and Fig. S1). The compounds were tested in human ovarian cancer cell lines OVCAR-8, NCI/ADR-RES, HEY, and OVCAR-3. Many of these compounds exhibited cytotoxicity with IC_{50} values below 10 μM (Table S1). It is important to note that the NCI/ADR-RES cell line shares a large number of karyotypic abnormalities with OVCAR-8 (21) but expresses high levels of MDR1 (multidrug resistance protein 1)/P-glycoprotein (22), resulting in resistance to multiple anticancer drugs in clinical use, including paclitaxel and doxorubicin. In addition, the human ovarian cancer cell line HEY is naturally resistant to cisplatin. Therefore, these results implicate our

Author contributions: S.X., N.A.P., and N.N. designed research; S.X., R.Y., Y.Z., B.D., R.D., and E.Z. performed research; A.N.B. contributed new reagents/analytic tools; S.X., Y.Z., B.D., N.A.P., and N.N. analyzed data; and S.X., N.A.P., and N.N. wrote the paper.

The authors declare no conflict of interest.

This article is a PNAS Direct Submission.

[1]To whom correspondence may be addressed. E-mail: petasis@usc.edu or neamati@usc.edu.

This article contains supporting information online at www.pnas.org/lookup/suppl/doi:10.1073/pnas.1205226109/-/DCSupplemental.

PACMA compounds' potential ability to overcome the current drug resistance issue in ovarian cancer therapy.

Active PACMA Analogs Covalently Bind to Their Cellular Target Protein in Human Ovarian Cancer Cells. Based on the electron-deficient nature of the propynoic acid amide moiety and confirmed by the structure–activity analysis (*SI Results*), we anticipated that the active PACMAs would be able to react irreversibly with certain nucleophilic groups, such as the thiol groups of cysteine side chains, to form covalent adducts. This property can be used to identify the protein target responsible for their activity and selectivity. To test this hypothesis, we first conjugated one of the most active analogs, **31**, to the fluorescent dye BODIPY (boron-dipyrromethene), resulting in **57**. We also synthesized **58**, a close analog of **57** that lacks the propynoyl group and is expected to be inactive, as well as the BODIPY compound **59** with acylated linker that can serve as the control (Fig. 1*A*). Fluorolog was used to determine the fluorescent properties of **57** (ex = 490 nm, em = 537 nm) (Fig. S2). The ability of **31**, **57**, **58**, and **59** to inhibit ovarian cancer cell growth was compared. PACMAs **31** and **57** exhibited similar potency (Fig. 1*B*), indicating that the conjugation of BODIPY to **31** did not affect the cytotoxic activity of **31**. No considerable cytotoxicity was observed with **58** or **59**, showing that the electrophilic alkyne is essential for potency and that the BODIPY moiety does not contribute to cytotoxicity. In addition, **57** and **58** displayed comparable fluorescent activity and were slightly less fluorescent than **59** (Fig. 1*C*), suggesting that the conjugations quenched the fluorescence of BODIPY only to a small extent.

To examine whether the active analog **57** covalently binds to its target protein, we treated OVCAR-8 cells with **57**, **58**, **59,** or equal amounts of DMSO. Cells were lysed after treatment and subjected to SDS/PAGE. A fluorescent band (~57 kDa) was only observed in the lane with **57**-treated samples (Fig. 1*D*). The interaction of **57** with its cellular protein target of ~57 kDa is covalent, because it was preserved under the denaturing conditions of the SDS/PAGE.

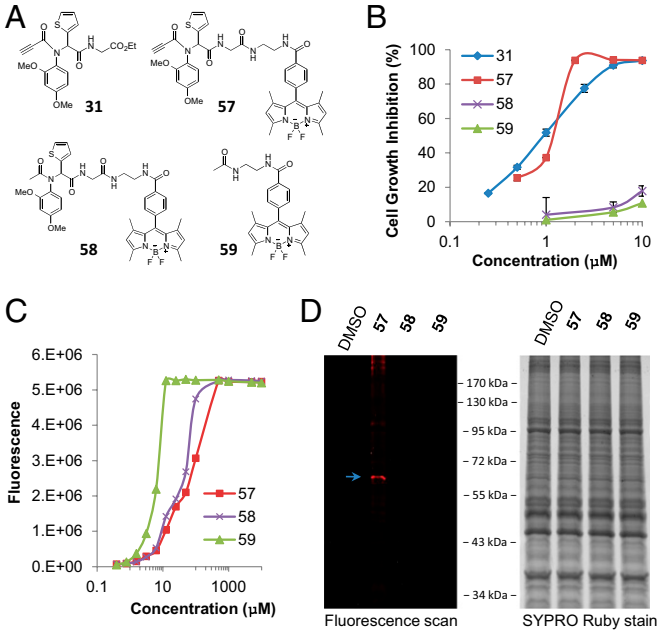

Fig. 1. BODIPY conjugation of PACMA **31**. (*A*) Structures of **31**, **57**, **58**, and **59**; (*B*) **31** and **57** but not **58** and **59** inhibited growth of OVCAR-8 cells as measured by MTT assay after 72 h treatment. Curves were generated from mean values (BAR, SEM). (*C*) BODIPY labeling of **57**, **58**, and **59** displays significant concentration-dependent fluorescence (λ_{ex} = 492 nm, λ_{em} = 535 nm). (*D*) PACMA **57** covalently binds to specific cellular proteins. Whole-cell lysates of OVCAR-8 cells treated with **57**, **58**, and **59** at 2 μM for 30 min were subjected to SDS/PAGE followed by fluorescence scan of BODIPY (*Left*) and SYPRO Ruby (*Right*). Arrow indicates a fluorescent band in **57**-treated cells. One of three representative experiments is shown.

Identification of PDI as the Target of PACMAs. To identify the 57-kDa protein, we performed 2D gel electrophoresis with whole-cell lysates from **57**-treated OVCAR-8 cells (Fig. 2*A*). Using MS, PDI was identified as a protein target of compound **57** (Fig. S3).

To confirm PDI as the target, we treated OVCAR-8 cells with **57**–**59** or DMSO. Whole-cell lysates were subjected to immunoprecipitation with anti-PDI antibody. A strong fluorescent band of ~57 kDa was detected only in the lane with **57**-treated OVCAR-8 cells (Fig. 2*B*), indicating that **57** covalently bound to PDI. In addition, subcellular colocalization of PDI and **57** was determined in OVCAR-8 cells using confocal microscopy (Fig. 2*C*). To evaluate whether the parent PACMA **31** binds to the same site in PDI as its fluorescent analog **57**, we performed a competition assay using purified recombinant PDI protein; **31** pretreatment blocked recombinant PDI protein from binding **57** (Fig. 2*D*), showing that the conjugation with BODIPY moiety does not change the target site of **31**. Fig. 2*E* shows that **57** binds to PDI protein in a time-dependent manner. The presence of DTT considerably increased this interaction (comparing lane 8 with lane 2), indicating that **57** targets free cysteine residues. Additionally, the binding of **57** to PDI is temperature-dependent (Fig. S4). We also evaluated the selectivity of the active analogs for PDI. After incubating **57** with an equal amount of PDI, BSA, or GRP78 (78-kDa glucose-regulated protein) core domain (another important molecular chaperone within the ER), we showed that **57** selectively binds to PDI, whereas no detectable fluorescence was observed from **57**-treated BSA or GRP78 core domain (Fig. 2*F* and Fig. S5). Together, these results indicate that the active PACMAs selectively target and covalently bind to PDI.

To identify the precise cysteine residues in PDI that form covalent bonds with **31**, online LC-Orbitrap CID (collision induced dissociation) and ETD (electron transfer dissociation) MS/MS were used (technical details are described in *SI Materials and Methods* and workflow for sample preparation and data analysis is shown in Fig. S6*A*). The addition of **31** led to a defined mass change of one peptide derived from the digestion of recombinant PDI protein that was directly measured by high-resolution MS with high confidence (Fig. S6*B*). This peptide fragment contains PDI's active site cysteines: C(397)GHC(400). The mass shift suggests that recombinant PDI was modified by **31** at either Cys397 or Cys400. Interestingly, Cys397 and Cys400 were not modified simultaneously, presumably because of steric hindrance caused by the binding of a PACMA **31** molecule. CID and ETD fragmentation MS/MS were also used to localize the modification site with single amino acid resolution. Detection of precursor ions at high resolution and a nearly complete series of fragmentation ions from both CID (Fig. S6*C*) and ETD (Fig. S6*D*) allowed the accurate sequencing and assignment of the modification site to Cys397/Cys400. Integrating all of the CID and ETD results, Protein Discoverer 1.3 automatically assigned potential modification sites at either Cys397 or Cys400 with high confidence (Fig. S6 *E* and *F*).

When **31** was docked on Cys397 of PDI using Protein Data Bank structure ID code 3UEM, we obtained a fitness score of 40.73, forming a covalent bond between the terminal carbon atom of the propynoic moiety of **31** and the sulfur atom of Cys397. We also observed two additional π–π interactions: one between **31**'s phenyl ring in R_1 and PDI's Trp396, and the other between **31**'s thienyl ring (R_2) and PDI's Phe304 (Fig. 3*A*). When **31** was docked on Cys400 of PDI, we obtained a fitness score of 33.53. PACMA **31** bound PDI through a covalent bond with Cys400 on the opposite side of the Cys397 site (Fig. 3*B*). In addition, **31**'s amide (-NH) formed a hydrogen bond with an oxygen within Pro395. We also

PHARMACOLOGY

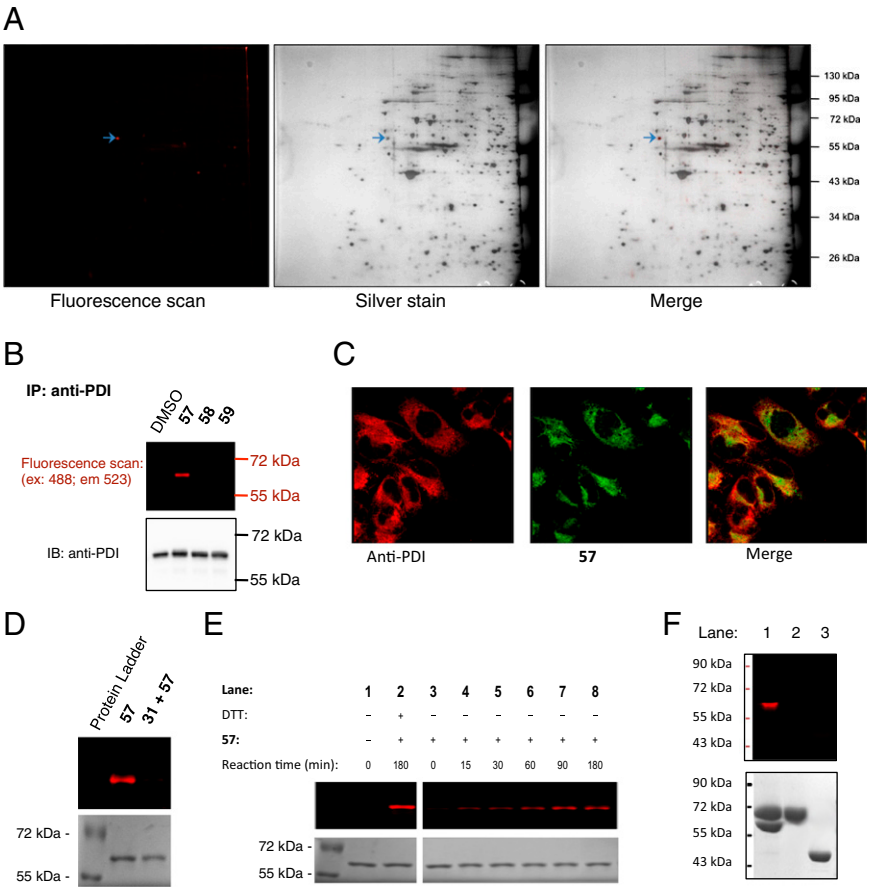

Fig. 2. PACMA **57** covalently binds to PDI. (*A*) Identification of PDI as the cellular protein target for **57**. OVCAR-8 cells were incubated with 2 μM **57** for 30 min. Whole-cell lysates were prepared as described for 2D gel electrophoresis (*SI Materials and Methods*), analyzed by isoelectric focusing/SDS/PAGE, scanned for BODIPY fluorescence (λ_{ex} = 488 nm, λ_{em} = 526 nm), and silver stained. The fluorescently tagged protein spot (arrow; ~57 kDa) was excised from the gel and analyzed by MS. (*B*) Immunoprecipitated cellular PDI was selectively and covalently bound by **57**. OVCAR-8 cells were incubated with **57**, **58**, and **59** at 2 μM for 30 min. Whole-cell lysates were subjected to immunoprecipitation using monoclonal anti-PDI antibody. Precipitated proteins were analyzed by SDS/PAGE and scanned for BODIPY fluorescence (*Upper*) followed by Western blotting with anti-PDI antibody (*Lower*). (*C*) Subcellular colocalization of PDI and **57**. OVCAR-8 cells were treated with 2 μM **57** for 30 min followed by fixation and permeabilization. Cellular PDI was stained with anti-PDI mAb. Subcellular localization of PDI and **57** was analyzed using confocal fluorescence microscopy. Red, PDI; green, **57**; yellow, merge. One of five representative microscope fields is shown. (*D*) Competition between **57** and **31** on PDI; 100 ng/μL recombinant PDI protein was incubated with 100 μM **31** or DMSO in sodium phosphate buffer (pH 7.0) for 1 h at 37 °C followed by 1 h incubation with 20 μM of **57**. Solutions were mixed with 5× SDS sample buffer and analyzed by SDS/PAGE, fluorescence scanning (*Upper*), and Coomassie Blue stain (*Lower*). (*E*) Kinetics study of covalent interaction between PDI and **57**; 100 ng/μL recombinant PDI was incubated with 20 μM **57** and/or 100 μM DTT for the indicated time at 37 °C followed by analysis using SDS/PAGE, fluorescence scanning (*Upper*), and Coomassie Blue staining (*Lower*). (*F*) PACMA **57** selectively bound to PDI; 20 μM **57** was incubated with 100 ng/μL recombinant PDI (lane 1; with 100 ng/μL BSA as a carrier protein), BSA (lane 2), or the core domain of GRP78 (lane 3) for 30 min at 37 °C followed by analysis using SDS/PAGE, fluorescence scan (*Upper*), and Coomassie Blue stain (*Lower*).

observed an extra π-cation interaction between **31**'s phenyl ring in R_1 and a side chain nitrogen of Lys401.

Active PACMAs Affect PDI Secondary Structure and Inhibit PDI Activity. Circular dichroism spectroscopy was performed to examine whether covalent binding of the active PACMAs to PDI would affect its secondary structure (23). Based on the circular dichroism data analysis using the K2D2 web server (www.ogic.ca/projects/k2d2/) (24), PACMAs **57** and **31** affected the secondary structure of PDI, whereas no substantial difference was observed between the spectra of recombinant PDI treated with vehicle control DMSO and the inactive analog **56** (Table 1 and Fig. S7*A*, representative curves). No substantial changes were observed in the secondary structure of the control protein BSA treated with **31**, **56**, or **57** (Table 1 and Fig. S7*B*, representative curves), indicating that covalent binding of active PACMAs to PDI affects its secondary structure.

Changes in protein structure are usually associated with variations in protein activity. PDI in the ER of mammalian cells is in the reduced state, allowing PDI to reduce and isomerize nonnative disulfide bonds of target proteins (25). We, therefore, examined the reductase activity of PDI with or without PACMA treatment in the insulin aggregation assay, a well-established assay for evaluating the activity of PDI (15); **31** significantly inhibited the activity of PDI in a dose- and time-dependent manner, producing complete inhibition at 100 μM (Fig. 4*A*). Direct comparison of **31** and phenylarsine oxide (PAO; a previously reported small-molecule PDI inhibitor) (26) (Fig. 4*B*) showed that **31** (IC_{50} of 10 μM) is a more potent PDI inhibitor than PAO (IC_{50} of 85 μM). However, **56** was inactive as expected (Fig. 4*C*). These results show that covalent binding of the active PACMAs to PDI inhibits its enzymatic activity.

Although PDI has been reported to play an important role in cancer progression (5, 12, 23, 27), it may be cancer- and cell type-specific. Therefore, we evaluated the viability of human ovarian cancer cells by silencing PDI. PDI siRNA substantially downregulated PDI expression in OVCAR-8 cells between 24 and 96 h (Fig. 5*A*). This finding was consistent with the significant inhibition of OVCAR-8 cell growth in the 3-(4,5-dimethylthiazol-2-yl)-2,5-diphenyltetrazolium bromide (MTT) assay (Fig. 5*B*).

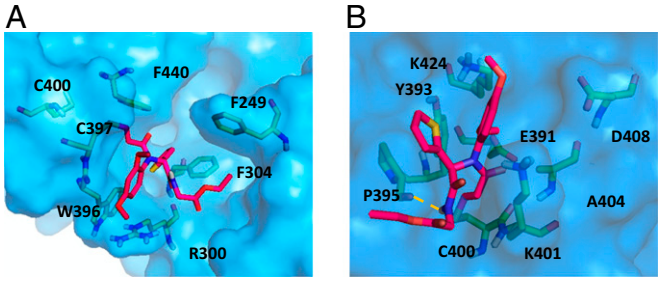

Fig. 3. PACMA **31** covalently binds to Cys397/Cys400 in PDI active site. Covalent docking of **31** (red) against PDI (blue; Protein Data Bank ID code 3UEM) with a covalent bond between the terminal carbon atom of **31**'s propynoic moiety and the sulfur atom of (*A*) Cys397 or (*B*) Cys400. Genetic Optimization for Ligand Docking fitness values are 40.73 and 33.53 for Cys397 and Cys400, respectively.

Table 1. Active PMCMAs affected PDI secondary structure

	DMSO	31	57	56
PDI				
α (%)	42.60	47.81	36.77	42.60
β (%)	9.77	8.18	12.31	9.77
BSA				
α (%)	84.27	84.27	84.27	84.27
β (%)	1.24	1.24	1.24	1.24

Additionally, silencing of PDI significantly inhibited colony formation by OVCAR-8 cells (Fig. 5*C*). Similarly, **31** significantly inhibited colony formation in OVCAR-8 cells in a dose-dependent manner (Fig. 5*D*). These results indicate that silencing of PDI is sufficient to cause considerable cytotoxicity in ovarian cancer cells.

PACMA 31 Suppresses Tumor Growth in Human Ovarian Cancer Mouse Xenografts. To evaluate the tumor targeting ability of active PACMAs in vivo, we tested **57**–**59** in a mouse xenograft model of human OVCAR-8 ovarian cancer. After 3 d of continuous i.p. administration, tumor, liver, and brain tissues were collected and prepared for frozen sections that were analyzed using fluorescent microscopy. PACMA **57**-treated tumor sections exhibited strong fluorescence intensity, whereas no fluorescence was detected in **58-** or **59**-treated tumor sections (Fig. 6*A*). Consistent with our in vitro data, one fluorescent band at ∼57 kDa was observed only in the **57**-treated tumor sample (Fig. 6*A*), confirming that PDI is covalently modified by **57** in the tumors. Because the liver is the major organ for drug metabolism, we also examined the fluorescent intensity in the liver of **57**–**59**-treated animals by fluorescence microscopy using the same settings and conditions used to examine the tumor sections. Compared with **57**-treated tumor sections, the liver sections of **57**-treated animals exhibited substantially lower fluorescent intensity (Fig. 6*A*). In comparison, liver sections from **58**-treated animals exhibited higher fluorescent intensity than liver sections from **57**-treated animals. No fluorescence emission was detected in **59**-treated liver sections as expected. In addition, no fluorescence emission was detected in brain sections with treatments of active or inactive compounds. Taken together, these data show that the active PACMAs selectively target and accumulate in ovarian tumors in vivo, and they do not cross the blood–brain barrier.

To determine the in vivo efficacy of **31**, we tested its effect on established tumors from OVCAR-8 cells through i.p. or *per os* administration; **31** was given i.p. at 20 mg/kg per day for the first 3 wk, with 5-d on and 2-d off treatment cycles. The dose was escalated to 40 mg/kg per day for the next 7 d. After 30-d i.p. treatment, the mouse xenografts were left untreated for an additional 32 d (Fig. S8). A second xenograft study was conducted to evaluate *per os* administration of **31**. Treatment was initiated with a dose of 20 mg/kg per day, and it was gradually increased by 20 mg/kg per day with each dose for 3 d before it was orally dosed at 200 mg/kg per day for an additional 32 d. The total duration of the oral treatment was 62 d (Fig. S8). Compared with the control group, i.p. or *per os* administration of **31** significantly inhibited tumor growth by 85% (from 796.6 to 117.0 mm^3, $P = 0.009$) and 65% (from 796.6 to 280.1 mm^3, $P = 0.015$) at day 62, respectively (Fig. 6*B*). Thus, **31** not only suppresses tumor growth in vivo but also is orally bioavailable. One mouse was found dead on day 30 in the i.p. administration group, but no obvious abnormalities were observed in other **31**-treated mice. The tumors in the i.p. treatment group did not aggressively grow after treatment was stopped on day 30. This finding may be at least partially because of the prolonged duration of drug action of **31**, a common feature of irreversible inhibitors. Compared with mice in the control group, no substantial body weight loss was detected in i.p. or *per os* groups during the study (Fig. S9*A*), indicating that **31** did not exert severe adverse effects on the mice at its effective anticancer dose. All mice were dissected at the end of the study (day 62). H&E staining of tumor sections showed extensive areas of necrosis in both **31** treatment groups (i.p. and *per os*) compared with the control group (Fig. 6*C*). In addition, no detectable abnormalities were observed in the organs examined, including liver, kidney, spleen, heart, lung, and pancreas (Fig. S9*B*), further showing the safety of PACMA **31**.

Discussion

In this study, we designed and synthesized a series of PACMAs that showed in vitro and in vivo anticancer activity in human ovarian cancer by targeting PDI. As a prototype of the ER protein disulfide isomerase family, PDI catalyzes the formation, cleavage, and rearrangement of disulfide bonds and facilitates oxidative protein folding by acting as a molecular chaperone (28). Therefore, PDI inhibition causes accumulation of unfolded or misfolded proteins that leads to ER stress and the unfolded protein response (UPR) that results in cell death (5). Compared with normal tissues, PDI is overexpressed in ovarian tumors (8). In addition, estrogen has been reported to increase PDI expression (29), bind PDI (30), and promote ovarian cancer progression (31). Based on these evidences, PDI is a promising drug target for ovarian cancer therapy.

We showed that inhibition of PDI by either small-molecule compounds or PDI siRNA resulted in substantial cytotoxicity in human ovarian cancer cells. Previously, it was shown that PDI knockdown results in apoptosis in human breast cancer MCF-7 cells and human neuroblastoma SH-SY5Y cells (32). Moreover, a PDI inhibitor, bacitracin, abrogated survival responses to ER stress and enhanced apoptosis caused by ER stress-inducing

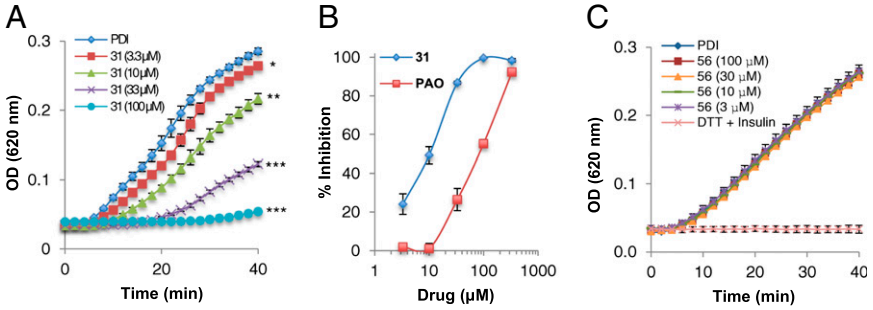

Fig. 4. Active PACMAs inhibit PDI activity. (*A*) PACMA **31** significantly inhibited the activity of PDI in a dose- and time-dependent manner in the insulin aggregation assay. Curves were generated from mean values (BAR, SEM). *$P < 0.05$; **$P < 0.01$; ***$P < 0.001$. (*B*) Comparison of the inhibitory activity of **31** and PAO. (*C*) PACMA **56** did not exhibit significant effects on the enzymatic activity of PDI. Experiments were performed in triplicate.

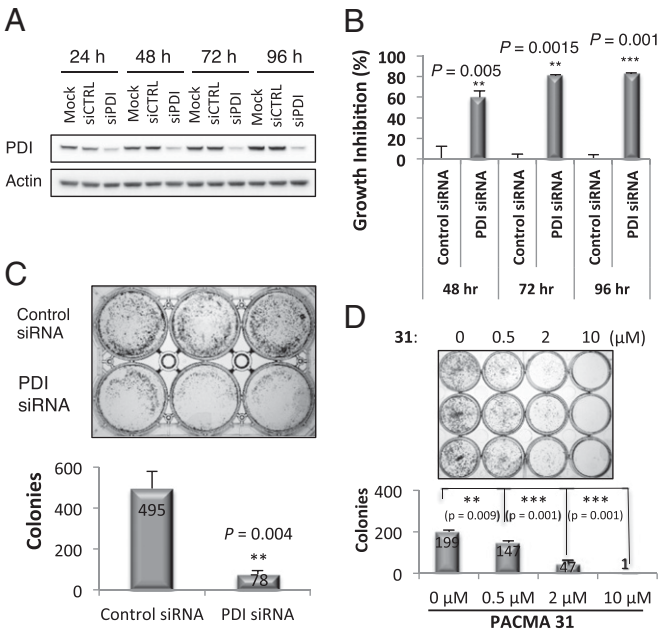

Fig. 5. Silencing of PDI inhibits cell growth of OVCAR-8 cells. (*A*) Representative Western blot of 24–96 h PDI silencing in OVCAR-8 cells. (*B*) PDI siRNA showed significant cytotoxicity as measured by MTT assay. The histogram shows the mean values of growth inhibition (%). (*C*) PDI knockdown significantly inhibited colony formation in OVCAR-8 cells. The histogram shows the mean number of colonies. (*D*) The 24-h treatment of **31** significantly inhibited the formation of OVCAR-8 colonies at indicated doses. The histogram shows the mean number of colonies (BAR, SEM). $^{**}P < 0.01$; $^{***}P < 0.001$.

agents, fenretinide and velcade, in human melanoma cells (5). In addition, both bacitracin and a PDI monoclonal antibody can inhibit migration and invasion of glioblastoma cells (12). However, the role of PDI in apoptosis might be cell type- and tissue-specific. It was documented that PDI knockdown by PDI siRNA has no significant effects on the viability of human cervical cancer HeLa cells (32). Therefore, PDI could be exploited as an important target for developing drugs against different cancers.

Irreversible drugs have proved to be successful therapies for various indications (33). To date, a large number of irreversible inhibitors have been reported to exhibit anticancer activities, such as α-difluoromethylornithine and covalent EGF receptor inhibitors (HKI-375, HKI-272, EKB569, BIBW2992, and PF299804) (34). Similar to the binding of irreversible inhibitors, post-translational modifications of PDI also suppress its enzymatic activity. Nitrosative stress-induced *S*-glutathionylation of PDI inhibits its enzymatic activity, leading to the activation of UPR and cell death in human ovarian cancer SKOV3 cells (23). Additionally, NO-induced *S*-nitrosylation of PDI down-regulates its enzymatic activity, resulting in the accumulation of polyubiquitinated proteins and the activation of UPR in neurodegenerative disorders (35).

The chemical structure of **31** suggests that it may be a prodrug, because it is possible that the ester bond can be hydrolyzed into an acid in vivo, converting **31** into **32** (Fig. S1). Because the activity of **31** is mostly dependent on the terminal acetamidoacetic acid moiety, this potential change does not cause loss of activity. This possibility is also supported by the activity of **32**, although it is less active (Table S1), probably because of the lower permeability of **32** caused by the negatively charged acidic group in solution.

PDI possesses two independent active sites: C(53)GHC(56) located within the α-domain and C(397)GHC(400) located within the α′-domain (36). Disruption of cysteines in either active site abolishes 50% of the catalytic activity of PDI, whereas disruption of cysteines in both active sites completely abolishes its catalytic activity (37). Using a liquid chromatography MS/MS method, we identified the PACMA **31** modification sites in the purified recombinant PDI protein as either Cys397 or Cys400, and both are located in the active C(397)GHC(400) site within

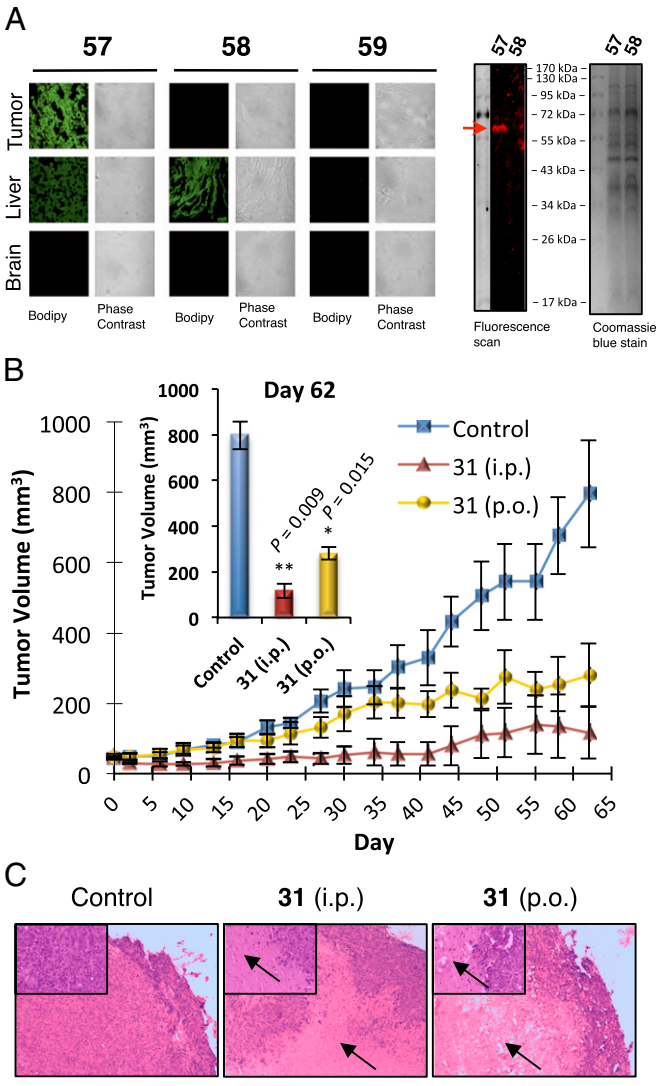

Fig. 6. PACMA **31** suppresses tumor growth in a mouse xenograft model of human OVCAR-8 ovarian cancer. (*A*) Mice were treated with **57**, **58**, and **59** at 10 mg/kg for 3 d with two injections per day; 6 h after the last injection, tumor, liver, and brain tissues were prepared for frozen sections and fluorescent microscopy analysis. (*Left*) Representative fluorescence images of indicated tissue sections captured using fluorescence microscopy and phase contrast. (*Right*) Gel fluorescence and Coomassie blue analysis of homogenized tumor samples from the **57**- and **58**-treated mice. An ~57-kDa fluorescent band in the **57**-treated tumor is indicated by a red arrow. (*B*) Growth curves of s.c. tumors in mice treated with **31** through i.p. (red; $n = 4$) or *per os* administration (yellow; $n = 4$) or treated with vehicle (blue; $n = 5$). Treatment schedules are described in Fig. S8. Results are presented as mean tumor volume (BAR, SEM). (*Inset*) Comparison of tumor volumes between control and **31** i.p. ($^{**}P < 0.01$) or **31** *per os* treatment group ($^{*}P < 0.05$) on day 62 (BAR, SEM). (*C*) PACMA **31** treatment induced extensive areas of necrosis in OVCAR-8 tumors. Representative images of H&E-stained tumor sections from control (*Left*) and **31**-treated (*Center*, i.p.; *Right*, *per os*) mice are shown. Arrows indicate areas of necrosis.

the α′-domain (Fig. S6 *B–F*). The location of these modification sites is consistent with the ability of **31** to inhibit the enzymatic activity of PDI. Additional modifications at Cys53 and Cys56 may occur in vivo because of the different redox environment in the ER, where these four cysteines should be in a reduced state that is required for full catalytic activity. In the recombinant PDI protein produced in *Escherichia coli*, a disulfide bond is probably formed between Cys53 and Cys56, which was shown in a PDI structure (Protein Data Bank ID code 1MEK) solved from a recombinant protein also produced in *E. coli* (38). Such a disulfide bond can protect Cys53/56 from PACMA **31** modification in vitro.

In summary, we identified PDI as a cellular protein target for PACMAs. We also showed that PDI knockdown in human ovarian cancer cells was cytotoxic and that our irreversible PDI inhibitors exhibited both in vitro and in vivo anticancer activity in human ovarian cancer models with tumor targeting ability and no substantial toxicity to normal tissues. Moreover, PACMAs were effective on human ovarian cancer cell lines resistant to conventional chemotherapy. Resistance to first-line therapy occurs in all ovarian cancer patients and is a major cause of mortality. Therefore, development of effective and safe PDI inhibitors as anticancer agents may overcome the current treatment failure in ovarian cancer therapy.

Materials and Methods

Measurement of PDI Activity. PDI activity was assayed by measuring the PDI-catalyzed reduction of insulin in the presence of DTT, thus measuring the aggregation of reduced insulin B chains at 620 nm as described previously (15). Briefly, recombinant PDI protein (0.4 μM) was incubated with indicated compounds at 37 °C for 1 h in sodium phosphate buffer (100 mM sodium phosphate, 2 mM EDTA, 8 μM DTT, pH 7.0). After this incubation, the modified recombinant PDI protein was added to the reaction mixture consisting of DTT (500 μM) and bovine insulin (130 μM; Sigma). The reduction reaction was catalyzed by PDI at room temperature, and the resulting aggregation of reduced insulin B chains was measured at 620 nm.

In Vivo Tumor Xenograft Studies. OVCAR-8 cells in logarithmic growth phase from cell culture were implanted in athymic mice (5×10^5 cells in 100 μL PBS/mouse) under aseptic conditions. Tumor growth was assessed by biweekly measurement of tumor diameters with a Vernier caliper (length × width). Tumor volume was calculated according to the formula tumor volume (in millimeters cubed) = $D \times d^2/2$, where D and d are the longest and shortest diameters, respectively. For i.p. administration, tumors were allowed to grow to an average volume of 50 mm^3. Mice were then randomly assigned into three groups: vehicle control ($n = 5$), i.p. treatment with **31** ($n = 4$; 20 mg/kg per day for the first 3 wk with 5-d on and 2-d off treatment cycles, and dose was escalated to 40 mg/kg per day for the next 7 d), and *per os* treatment of **31** ($n = 4$; the initial dose of 20 mg/kg per day was gradually increased by 20 mg/kg per day with each dose for 3 d before it was orally dosed at 200 mg/kg per day for an additional 32 d, increasing the dose from 20 to 200 mg/kg). Treatment schedules are described in Fig. S8. Treatment of each animal was based on individual body weight. The body weights and tumor volumes in each group were measured two times per week. The percentage of tumor growth inhibition was calculated as *T/C*% = 100 × (mean *TW* of treated group)/(mean *TW* of control group).

Additional reagents and procedures used in this report are described in detail in *SI Materials and Methods*.

ACKNOWLEDGMENTS. This work was supported in part by the University of Southern California Zumberge Research and Innovation Fund, the Arthur C. Cope Scholar Fund administered by the American Chemical Society (N.A.P.), and the Sharon and William Cockrell Endowed Cancer Research Fund (N.N.) and Department of Defense Ovarian Cancer Program (W81XWH-07-1-0414) Idea Award (N.N).

1. Siegel R, Naishadham D, Jemal A (2012) Cancer statistics, 2012. *CA Cancer J Clin* 62: 10–29.
2. Petty R, Evans A, Duncan I, Kurbacher C, Cree I (1998) Drug resistance in ovarian cancer—the role of p53. *Pathol Oncol Res* 4:97–102.
3. Hatahet F, Ruddock LW (2009) Protein disulfide isomerase: A critical evaluation of its function in disulfide bond formation. *Antioxid Redox Signal* 11:2807–2850.
4. Hoffstrom BG, et al. (2010) Inhibitors of protein disulfide isomerase suppress apoptosis induced by misfolded proteins. *Nat Chem Biol* 6:900–906.
5. Lovat PE, et al. (2008) Increasing melanoma cell death using inhibitors of protein disulfide isomerases to abrogate survival responses to endoplasmic reticulum stress. *Cancer Res* 68:5363–5369.
6. Gruber CW, Cemazar M, Heras B, Martin JL, Craik DJ (2006) Protein disulfide isomerase: The structure of oxidative folding. *Trends Biochem Sci* 31:455–464.
7. Haefliger S, et al. (2011) Protein disulfide isomerase blocks CEBPA translation and is up-regulated during the unfolded protein response in AML. *Blood* 117:5931–5940.
8. Bonome T, et al. (2008) A gene signature predicting for survival in suboptimally debulked patients with ovarian cancer. *Cancer Res* 68:5478–5486.
9. Welsh JB, et al. (2001) Analysis of gene expression identifies candidate markers and pharmacological targets in prostate cancer. *Cancer Res* 61:5974–5978.
10. Beer DG, et al. (2002) Gene-expression profiles predict survival of patients with lung adenocarcinoma. *Nat Med* 8:816–824.
11. Basso K, et al. (2005) Reverse engineering of regulatory networks in human B cells. *Nat Genet* 37:382–390.
12. Goplen D, et al. (2006) Protein disulfide isomerase expression is related to the invasive properties of malignant glioma. *Cancer Res* 66:9895–9902.
13. Rickman DS, et al. (2001) Distinctive molecular profiles of high-grade and low-grade gliomas based on oligonucleotide microarray analysis. *Cancer Res* 61:6885–6891.
14. Talantov D, et al. (2005) Novel genes associated with malignant melanoma but not benign melanocytic lesions. *Clin Cancer Res* 11:7234–7242.
15. Khan MM, et al. (2011) Discovery of a small molecule PDI inhibitor that inhibits reduction of HIV-1 envelope glycoprotein gp120. *ACS Chem Biol* 6:245–251.
16. Dickerhof N, Kleffmann T, Jack R, McCormick S (2011) Bacitracin inhibits the reductive activity of protein disulfide isomerase by disulfide bond formation with free cysteines in the substrate-binding domain. *FEBS J* 278:2034–2043.
17. Wang EJ, Snyder RD, Fielden MR, Smith RJ, Gu YZ (2008) Validation of putative genomic biomarkers of nephrotoxicity in rats. *Toxicology* 246:91–100.
18. Weston BS, Wahab NA, Roberts T, Mason RM (2001) Bacitracin inhibits fibronectin matrix assembly by mesangial cells in high glucose. *Kidney Int* 60:1756–1764.
19. Godin B, Touitou E (2004) Mechanism of bacitracin permeation enhancement through the skin and cellular membranes from an ethosomal carrier. *J Control Release* 94:365–379.
20. Yamada R, et al. (2011) Discovery and preclinical evaluation of a novel class of cytotoxic propynoic acid carbamoyl methyl amides (PACMAs). *J Med Chem* 54:2902–2914.
21. Roschke AV, et al. (2003) Karyotypic complexity of the NCI-60 drug-screening panel. *Cancer Res* 63:8634–8647.
22. Alvarez M, et al. (1995) Generation of a drug resistance profile by quantitation of mdr-1/P-glycoprotein in the cell lines of the National Cancer Institute Anticancer Drug Screen. *J Clin Invest* 95:2205–2214.
23. Townsend DM, et al. (2009) Nitrosative stress-induced s-glutathionylation of protein disulfide isomerase leads to activation of the unfolded protein response. *Cancer Res* 69:7626–7634.
24. Perez-Iratxeta C, Andrade-Navarro MA (2008) K2D2: Estimation of protein secondary structure from circular dichroism spectra. *BMC Struct Biol* 8:25.
25. Feige MJ, Hendershot LM (2011) Disulfide bonds in ER protein folding and homeostasis. *Curr Opin Cell Biol* 23:167–175.
26. Root P, Sliskovic I, Mutus B (2004) Platelet cell-surface protein disulphide-isomerase mediated S-nitrosoglutathione consumption. *Biochem J* 382:575–580.
27. Fonseca C, et al. (2009) Protein disulfide isomerases are antibody targets during immune-mediated tumor destruction. *Blood* 113:1681–1688.
28. Noiva R (1999) Protein disulfide isomerase: The multifunctional redox chaperone of the endoplasmic reticulum. *Semin Cell Dev Biol* 10:481–493.
29. Ejima K, et al. (1999) 17beta-estradiol induces protein thiol/disulfide oxidoreductases and protects cultured bovine aortic endothelial cells from oxidative stress. *Eur J Endocrinol* 140:608–613.
30. Primm TP, Gilbert HF (2001) Hormone binding by protein disulfide isomerase, a high capacity hormone reservoir of the endoplasmic reticulum. *J Biol Chem* 276:281–286.
31. Spillman MA, et al. (2010) Tissue-specific pathways for estrogen regulation of ovarian cancer growth and metastasis. *Cancer Res* 70:8927–8936.
32. Hashida T, Kotake Y, Ohta S (2011) Protein disulfide isomerase knockdown-induced cell death is cell-line-dependent and involves apoptosis in MCF-7 cells. *J Toxicol Sci* 36:1–7.
33. Singh J, Petter RC, Baillie TA, Whitty A (2011) The resurgence of covalent drugs. *Nat Rev Drug Discov* 10:307–317.
34. Jänne PA, et al. (2011) Phase I dose-escalation study of the pan-HER inhibitor, PF299804, in patients with advanced malignant solid tumors. *Clin Cancer Res* 17: 1131–1139.
35. Uehara T, et al. (2006) S-nitrosylated protein-disulphide isomerase links protein misfolding to neurodegeneration. *Nature* 441:513–517.
36. LaMantia ML, Lennarz WJ (1993) The essential function of yeast protein disulfide isomerase does not reside in its isomerase activity. *Cell* 74:899–908.
37. Vuori K, Myllylä R, Pihlajaniemi T, Kivirikko KI (1992) Expression and site-directed mutagenesis of human protein disulfide isomerase in Escherichia coli. This multifunctional polypeptide has two independently acting catalytic sites for the isomerase activity. *J Biol Chem* 267:7211–7214.
38. Kemmink J, Darby NJ, Dijkstra K, Nilges M, Creighton TE (1996) Structure determination of the N-terminal thioredoxin-like domain of protein disulfide isomerase using multidimensional heteronuclear 13C/15N NMR spectroscopy. *Biochemistry* 35: 7684–7691.